

## Application of impedance imaging to evaluation of organic coating degradation at a local scale

M. Szociński, K. Darowicki, K. Schaefer

© The Author(s) 2012. This article is published with open access at Springerlink.com

**Abstract** A new approach for evaluating the local electrical properties of organic coatings has been proposed. It was performed with contact mode atomic force microscopy (AFM). A current response signal was measured when a single-frequency voltage perturbation was applied between AFM tip and coated metal. Suitability of the proposed technique has been presented on the representative acrylic coating degraded by two different factors—UV radiation and electrolyte exposure. It was possible to disclose the early stages of the coating deterioration, to spatially localize defective regions, and to observe distinctly different modes of the coating degradation as a result of exposure to various degradation factors.

**Keywords** Organic coatings, Polymer, AFM, EIS, Paint coatings

### Introduction

Performance of a protective organic coating depends on the performance of its weakest component. It is usually some local region of the protective film, which fails when exposed to particular conditions. It becomes a site of damage onset and a starting point of degradation progress. Assessing the degradation mode of a particular coating as well as identifying the areas responsible for degradation initiation is a matter of vital importance from a paint manufacturer's point of view. Being able to reveal whether the weakest point is the polymer resin

matrix, pigment, or pigment/matrix interface can result in valuable information for paint chemists, indicating the potential areas requiring improvement. In order to obtain such information a suitable measurement technique capable of providing localized results must be employed.

Taylor and Moongkhamklang utilized fluorescence microscopy to address the issue that has not been solved by the local electrochemical methods: whether the transport of water and ions occurs via discrete or regional heterogeneities within an epoxy coating or whether these species enter as a uniform front.<sup>1,2</sup> The effect of relative humidity on moisture-enhanced photolysis of acrylic-melamine coatings was investigated by Nguyen et al. using Fourier transform infrared spectroscopy (FTIR) and yielding complex and structure-specific degradation due to inherently heterogeneous microstructure of the coating.<sup>3</sup> Further studies on the mode and mechanism of hydrolytic degradation of acrylic-melamine coatings were described by Nguyen et al.<sup>4</sup> Insufficient performance of artificially weathered navy coating systems due to impaired polydispersity of one of the coating components was revealed by Keene et al. who used FTIR, X-ray photoelectron spectroscopy (XPS) imaging and optical and scanning electron microscopy–energy dispersive spectroscopy (SEM–EDS) as well as laser-confocal topography.<sup>5</sup> Souto et al. contributed to identification of early stages of coating degradation by SEM investigation of blistering phenomenon upon exposure to aqueous solutions of various salts.<sup>6–9</sup> Atomic force microscopy (AFM) method has also turned out to be a useful tool in evaluating a polymer film's heterogeneity. Raghavan et al. applied the AFM to study thin film blends of polystyrene and polybutadiene as a function of annealing time at elevated temperature<sup>10</sup> as well as the multiphase polyethyl acrylate/polystyrene blend exposed to a hydrolytic acidic environment.<sup>11</sup> In these investigations the AFM proved to be valuable for quantitative study of pit formation and growth in the

---

M. Szociński (✉), K. Darowicki, K. Schaefer  
Department of Electrochemistry, Corrosion and Materials  
Engineering, Chemical Faculty, Gdansk University  
of Technology, 11/12 G. Narutowicza Str.,  
Gdańsk 80-233, Poland  
e-mail: micszoci@chem.pg.gda.pl

coating as well as for identification of particular phase domains. Electrochemical impedance spectroscopy (EIS) is also a popular tool in the field of organic coatings.<sup>12–18</sup> However, the investigated region typically engulfs the area of a few centimeters<sup>2</sup> and thus the results are significantly averaged and provide no or little information about local characteristics of the protective film. To overcome that disadvantage the authors of the paper employed the methodology originally proposed by Kalinin and co-workers for investigation of transport behavior of individual grains and grain boundaries in polycrystalline ZnO<sup>19</sup> and then also used by O’Hayre in the field of solid polymer electrolytes, polycrystalline ZnO varistors and micro-scale test patterns characterized by distinctly different electrical behavior.<sup>20,21</sup> It enables local impedance imaging and spectroscopy to be performed along with contact AFM measurements. During the AFM scan (imaging) or at a fixed stationary location of a tip (spectroscopy), an AC voltage perturbation signal is applied between the AFM tip and investigated sample and an AC current response signal is registered providing local electrical characteristics of examined material. Fundamentals and details of the application of this technique to investigate organic coatings have been described by Darowicki et al.<sup>22</sup>

In this approach impedance is determined in a two-electrode system: the conductive AFM tip and investigated sample, for instance, metal substrate protected with organic coating. A single-frequency voltage perturbation signal is set between the electrodes and the current response signal is recorded. Thus, one is capable of mapping impedance of the scanned area.

The resolution of this method is dependent on such factors as: the size of the AFM tip, frequency of the perturbation signal and the scan rate.

The smaller radius of the AFM tip the higher resolution and impedance response is confined to the material volume directly adjacent to the tip/sample contact point. However, small contact area means high impedance that is difficult to measure. Accordingly, in the case of thick barrier coatings these are rather relative changes of impedance as a function of tip position, rather than absolute impedance values that are measured.

Dielectric materials such as organic barrier coatings require high frequencies and amplitude perturbation. For dielectric materials the current response signal to a sinusoidal voltage perturbation is described by the formula:

$$\Delta I \approx j\omega C \Delta E \quad (1)$$

where  $\omega$  is the signal frequency,  $\Delta E$  is the signal amplitude, and  $C$  is the material capacitance. AC response possesses imaginary character for relatively high frequency. Thus, for dielectrics, the response is capacitive.

Low impedance systems require perturbation of lower frequency and amplitude. In this case the response signal is given by the formula:

$$\Delta I \approx \frac{1}{R} \Delta E \quad (2)$$

where  $\omega$  is the signal frequency,  $\Delta E$  is the signal amplitude, and  $R$  is the material resistance.

Another parameter influencing measurement resolution is the scan rate. For a constant scan rate the application of a relatively high measurement frequency yields high spatial resolution. Such an approach is well suited for dielectric materials. Samples of resistive character demand perturbation of relatively low frequency. Thus, in order to obtain high spatial resolution of such measurements, one has to decrease the scan rate.

This article presents the suitability of this localized variant of impedance measurement for revealing different modes of organic coating degradation while exposed to UV radiation and electrolyte immersion, respectively.

## Experimental

The samples subjected to investigation consisted of acrylic coating applied on circular carbon steel substrate (1 mm diameter) by air spray technique (Fig. 1). The coating thickness, measured using electronic thickness gauge, Phynix Surfex, was equal to  $20 \pm 3 \mu\text{m}$ . The roughness of steel substrate was  $12 \mu\text{m}$  in terms of  $R_{y5}$  parameter.

Coating degradation was induced in two ways: the first set of samples was subjected to an immersion in 3% sodium chloride (NaCl) solution for 400 h; the second set of specimens was exposed to UV irradiation for 900 h (UV radiation was generated by a 320 nm wavelength lamp providing the radiation intensity of  $3.6 \text{ W/m}^2$  at a distance of 1 m). In both cases classical and localized impedance measurements were carried out at regular time intervals during the exposure in order to assess the condition and extent of coating degradation.

A two-electrode system with the substrate as a working electrode and platinum mesh as a counter electrode was employed in classical impedance measurements on a global scale (Fig. 2). The investigation was performed upon immersion in 3% sodium chloride solution. The examined area was  $0.8 \text{ mm}^2$ . The experimental set-up included the Schlumberger 1255 frequency response analyzer with the high input

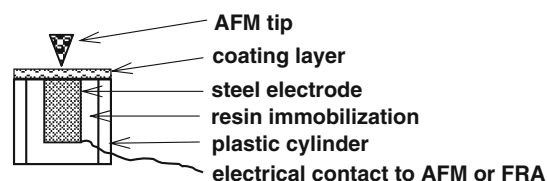


Fig. 1: Scheme of a cross section of the specimen for AFM investigations

impedance buffer Atlas 9181. Measurement frequency range was from 1 MHz to 1 mHz. Ten points were recorded for each frequency decade. An amplitude of the perturbation signal was equal to 120 mV, which was selected experimentally based on a series of impedance measurements, each with different amplitude of the perturbation. The amplitude of 120 mV provided stability and improved signal-to-noise ratio at the same time.

Localized electrical and topographic measurements were accomplished with the SPM Ntegra Aura system by NT-MDT Co. Each classical impedance measurement was followed by AFM investigation in contact mode. The samples were dried in laboratory conditions for 12 h before every AFM examination. Ten locations distributed over the surface of the specimen were examined for reproducibility of the results.

The height profile, local impedance, and spreading resistance images were taken for every location. Height and local impedance images were taken simultaneously, while spreading resistance was taken during the second pass. Scanning by the tip mode was employed, allowing investigation of the maximum area of  $8100 \mu\text{m}^2$  ( $90 \mu\text{m} \times 90 \mu\text{m}$ ). The resolution of measurement was  $0.35 \mu\text{m}$  (scanned distance  $90 \mu\text{m}$  divided by a number of pixels in a line—256). For each specimen the maximum area was scanned at first for a general overview and then more area-confined scans in the places of interest were collected. All the scans were obtained for the set point providing the contact force of  $6 \mu\text{N}$ , which yielded satisfactory topographic images as well as stable electrical contact during electrical measurements. As far as the local AC measurements were concerned, while scanning a single-frequency sinusoidal voltage signal of 3 kHz was applied between the tip

and the steel substrate and the current response of the sample was registered by lock-in amplifier incorporated in the Ntegra Aura system. Perturbation signal amplitude was 2 V. Additionally, spreading resistance measurements were performed with a DC bias voltage within the range 2–10 V. In each case scanning frequency was equal to 1 Hz. The silicon AFM tip coated with platinum was used, the parameters of which are presented in Table 1. Nova software by NT-MDT Co. was employed for image registration, processing, and analysis.

## Results and discussion

An initial state of the coating was characterized by the AFM and EIS investigation. Figure 3a presents a topographic image of the coating surface prior to an exposure to electrolyte solution or UV radiation. There are some hills and valleys visible and the maximum difference in height between these does not exceed  $3 \mu\text{m}$ . Localized impedance characteristics obtained using the AFM-based set-up reveal strong correlation with the topography. In Fig. 3b the amplitude of the AC current response signal is inversely proportional to the height profile—the elevated areas correspond to low amplitude of the AC response signal, while the depressed regions are characterized by higher AC response current amplitude. For a relatively high amplitude of the AC perturbation voltage (3 kHz) the response signal describes capacitive properties of the investigated coating.<sup>22</sup> Coating capacitance is described by the formula:

$$C = \frac{\varepsilon\varepsilon_0 A}{d} \quad (3)$$

where  $\varepsilon$  is the dielectric permittivity of coating material,  $\varepsilon_0$  is the dielectric permittivity of vacuum,  $A$  is the area exposed to investigation, and  $d$  denotes the coating thickness. An inverse proportionality between coating thickness and capacitance and thus registered current is evident. Scanning spreading resistance measurements employing a DC signal did not reveal any breakthrough defects of the coating. Excellent initial barrier properties of the coating were also confirmed by the global EIS measurements (Fig. 3c). A global impedance spectrum exhibits one time constant and describes the coating/substrate system of a few hundred M $\Omega$  resistance.

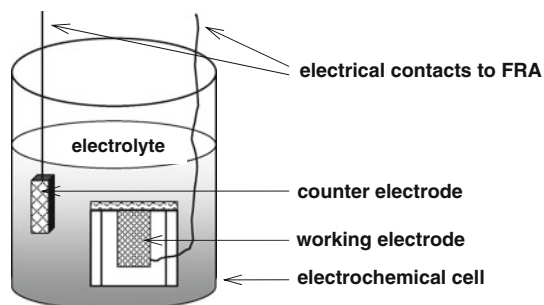


**Fig. 2: Scheme of a set-up for global impedance measurements**

**Table 1: Parameters of the tip CSG10/Pt by NT-MDT utilized in the investigations**

Chip size (mm)	Tip height ( $\mu\text{m}$ )	Tip curvature radius (nm)	Tip side coating	Cantilever length ( $\mu\text{m}$ )	Cantilever width ( $\mu\text{m}$ )	Cantilever thickness ( $\mu\text{m}$ )	Resonant frequency (kHz)	Force constant (N/m)
$3.4 \times 1.6 \times 0.3$	14–16	15–20	Pt 20 nm	225	30	0.5–1.5	8–39	0.01–0.5

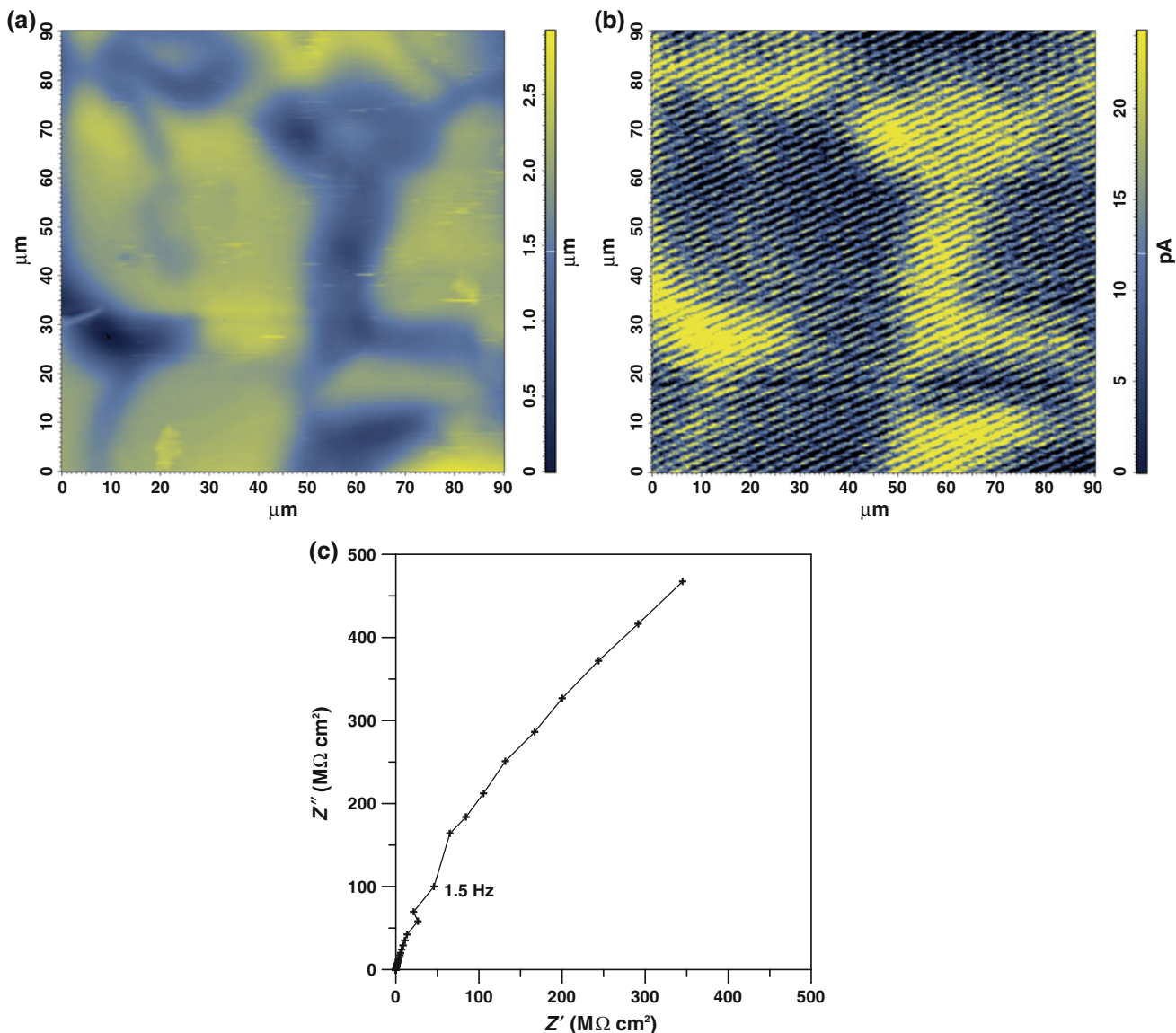


**Fig. 3: Exemplary AFM height image (a) and impedance image (AC current response amplitude) (b) and global impedance spectrum (c) of the coating prior to the investigation**

The exposure to both hostile environments resulted in an onset of coating’s degradation. However, these early stages of degradation could be elucidated only from the AFM-based measurements (Figs. 4, 5). Topography and AC current response images provided evidence of some cracks that appeared on the investigated surfaces, constituting the potential sites where damage started. Spreading resistance measurements did not provide any evidence of through-the-coating defects. Thus the visible cracks did not penetrate the entire bulk of the coating, but contributed to an increased surface roughness as compared to the initial one, especially in the case of the UV-exposed sample (maximum difference in height profile is about 4 μm). Such information is inaccessible via the global impedance measurement, where the spectra registered after

the analogous period of time still revealed one time constant and high resistance of the film suggesting stable, excellent barrier properties. In addition, only localized measurements allowed for the differentiation of the modes of degradation of the same coating in different environments. In Fig. 4a, b it is evident that the microcracks, which formed on the coating surface after the exposure to electrolyte start from the very top of the elevated regions. A possible explanation for this mode of degradation is preferential electrolyte ingress into susceptible regions of the coating. The absorbed electrolyte contributed to minor blistering of the coating and exerted pressure on a surface layer of the protective film. As the local tensile strength of the coating had been exceeded, the crack formed at the blister’s apex and consequently propagated through

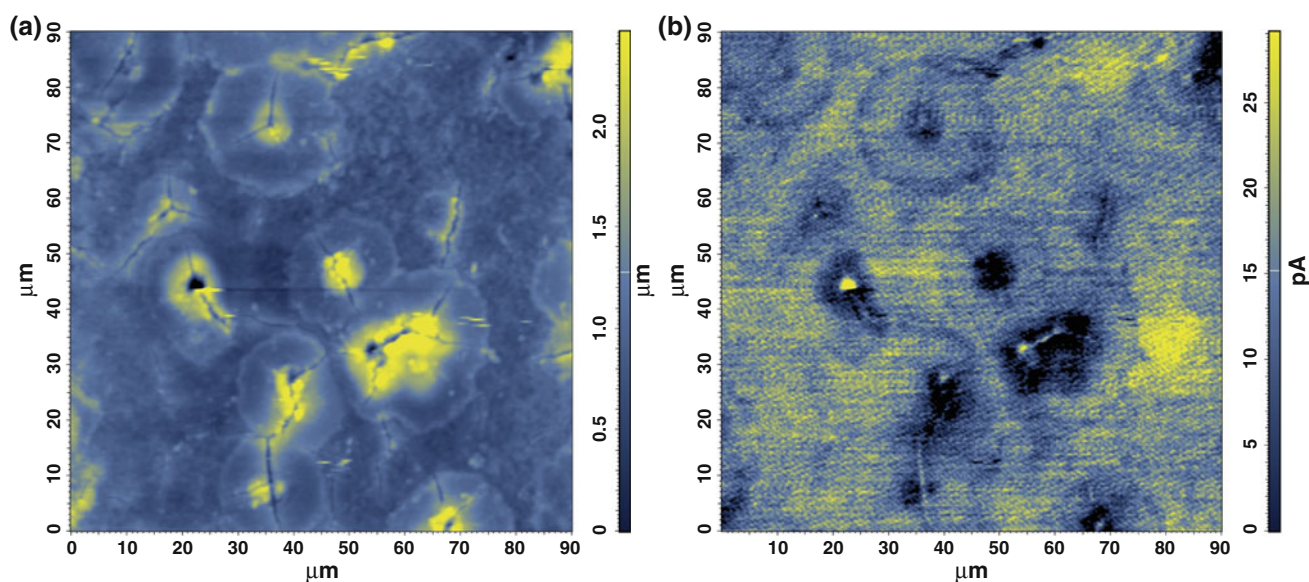


Fig. 4: Exemplary AFM height image (a) and impedance image (AC current response amplitude) (b) of the coating after 250 h of immersion in 3% NaCl solution

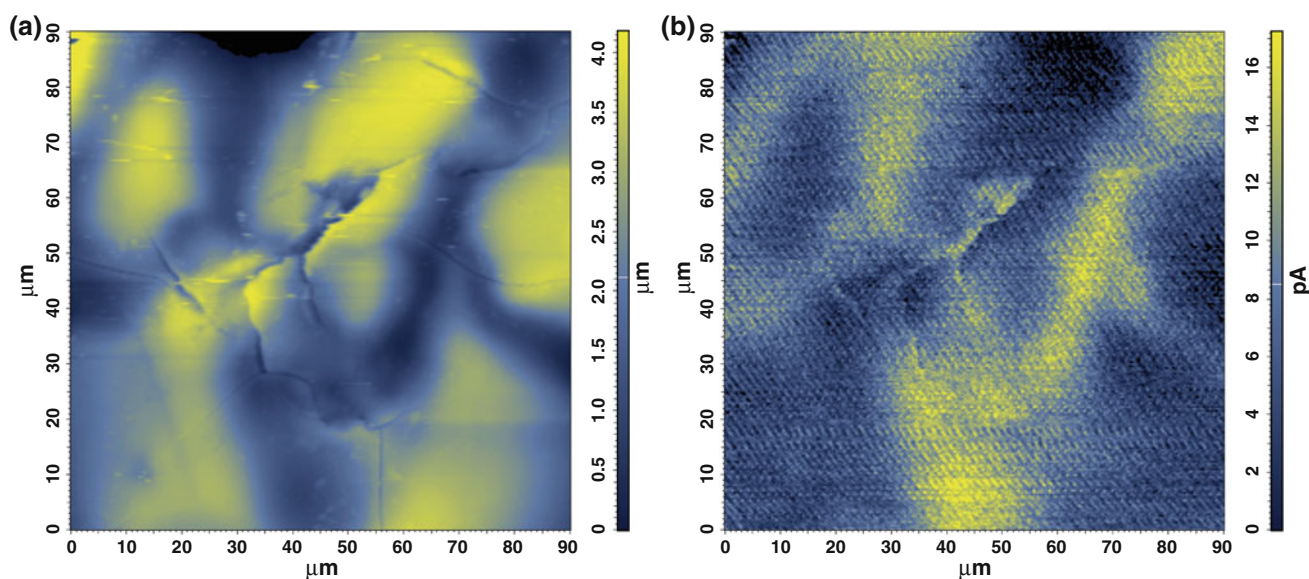
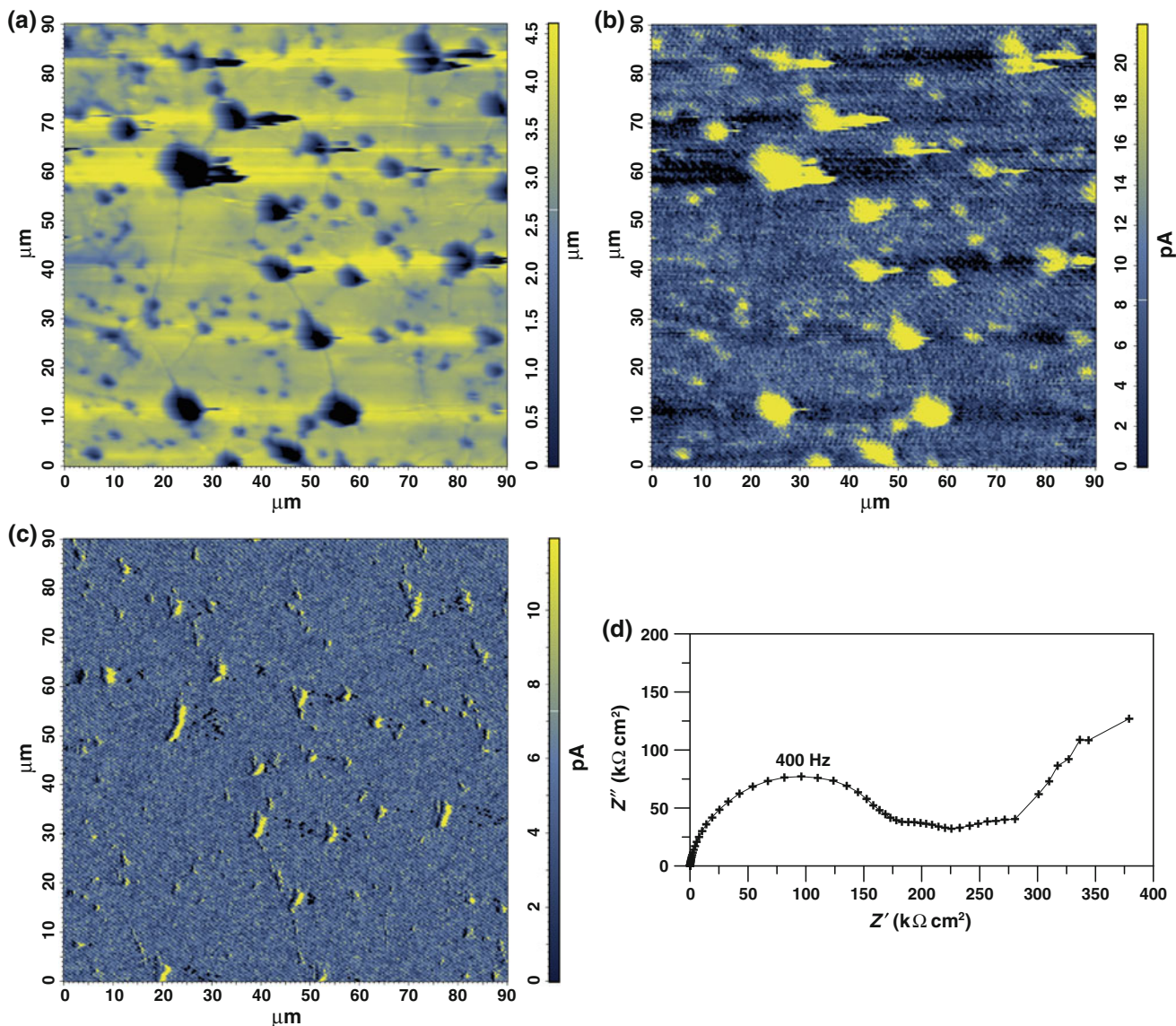


Fig. 5: Exemplary AFM height image (a) and impedance image (AC current response amplitude) (b) of the coating after 600 h of exposure to UV radiation

the material. The points of crack initiation were probably the weakest areas of the coating, which could not withstand electrolyte attack upon exposure. They do not correspond to the highest points of the profile prior to electrolyte exposure as there is no such correlation that can be seen from the AFM images. Rather, these are the spots with poor crosslinking, impaired adhesion, imperfect application or with random defects such as dust particles incorporated in wet polymer film. These could also be the sites of reduced coating thickness over the substrate roughness profile. Relatively developed surface of the substrate

( $R_{y5} = 12 \mu\text{m}$ ) as compared to the coating thickness (av.  $20 \mu\text{m}$ ) could result in weaker protection of the selected profile peaks, which frequently happens to be the reason for premature coating failure in practice. Those regions were revealed after a certain period of immersion time, which is consistent with the mechanism of blister formation.<sup>23</sup> Due to the concentration gradient between a cavity inside/underneath the coating and electrolyte bulk, the electrolyte is gradually pumped from the bulk inside. As a result a blister develops and elevates the coating locally. The tensile stress at the apex of the blister is the highest and causes cracking of the coating



**Fig. 6: Exemplary AFM height image (a), impedance image (AC current response amplitude) (b), spreading resistance image (c), and global impedance spectrum (d) of the coating after 400 h of immersion in 3% NaCl solution**

layer there. Finally, the blister opens, allowing for the electrolyte ingress and the cracks propagation in random directions away from the blister.

A different mechanism of degradation is revealed by the same acrylic coatings, but that has been exposed to UV radiation (Fig. 5a, b). There were no blisters found on the investigated coating and it gradually became covered with a mesh of tiny cracks running randomly over the specimen’s surface. Accordingly, it was the entire area that suffered from the UV effect, and the energy carried with the radiation contributed to polymer chain bond scission at numerous locations, which then combined into the net of cracks.

It is due to the localized topographic and electrical measurement that such different modes of degradation of the same coating could be distinguished. Global

impedance measurement provided only averaged information about the coating state, which did not give any indication of degradation onset, not to mention the mode of failure.

The results of coating exposure to 400 h of immersion in 3% sodium chloride solution and 900 h of UV radiation are presented in Figs. 6 and 7, respectively. Localized measurements reveal advanced degradation of the coating and confirm that previously observed cracks were indeed the sites of coating degradation onset. At this stage of the exposure it can be seen from scanning spreading resistance measurements (Figs. 6c, 7c) that the cracks transformed into through-the-coating defects reaching the metal substrate, which do not constitute a barrier for DC current. The defective nature of the coatings was confirmed by the global

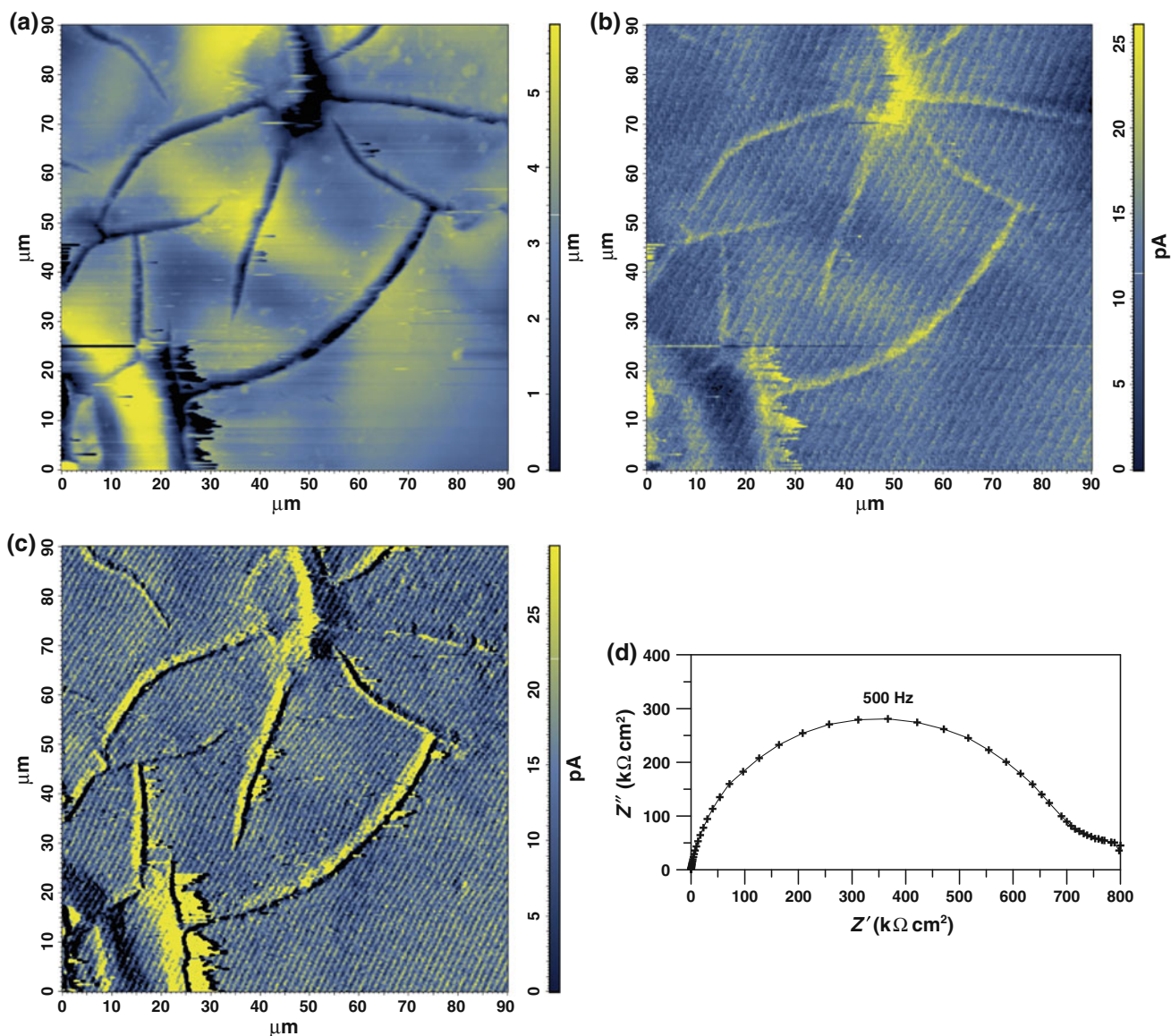


**Fig. 7:** Exemplary AFM height image (a), impedance image (AC current response amplitude) (b), spreading resistance image (c), and global impedance spectrum (d) of the coating after 900 h of exposure to UV radiation

impedance measurements. The spectra registered at the end of exposure (Figs. 6d, 7d) showed the resistance of the coatings of a few hundred  $k\Omega$  order, which is below the threshold level of  $M\Omega$  considered a border between a protective barrier coating and a defective one.<sup>24</sup> In the case of electrolyte exposure, a low-frequency semicircle is also visible, indicating an electrochemical reaction at the metal substrate.

## Conclusions

Based on the performed investigations the following conclusions can be drawn:

- The presented contact mode AFM-based technique of local impedance and electrical characterization of organic coatings enabled differentiation and description of diverse modes of acrylic film degradation upon exposure to different environments.
- The approach applied yielded the results, which not only were consistent with the classical impedance measurements performed on a global scale but also provided information inaccessible by the classical impedance technique, namely early identification of potential sites of coating degradation onset, mode of coating degradation, and spatial localization of defects.
- As opposed to the classical EIS measurements, the technique utilized in the present studies does not

require the presence of electrolyte, which facilitates measurement procedure and gives more reliable results of coatings' testing, which are not meant to serve in wet or high moisture environments.

- The described method of localized impedance investigation is of significant application potential in the fields requiring both detection of discrete, tiny defects in protective coatings (for example, in the coatings on printed boards in electronic industry) and identification of the sites and coating regions particularly susceptible to degradation (for instance, during verification of new coating formulation performance in various environments).

**Acknowledgments** The authors acknowledge the financial support for this study by the Grant No. N 204 501 739 from the Polish Ministry of Science and Higher Education.

**Open Access** This article is distributed under the terms of the Creative Commons Attribution License which permits any use, distribution, and reproduction in any medium, provided the original author(s) and the source are credited.

## References

1. Taylor, SR, Moongkhamklang, P, "The Delineation of Local Water Interaction with Epoxy Coatings Using Fluorescence Microscopy." *Prog. Org. Coat.*, **54** 205–210 (2005)
2. Moongkhamklang, P, Taylor, SR, "The Delineation of Ionic Pathways in Organic Coatings Using a Molecular Probe Technique." *Prog. Org. Coat.*, **46** 259–265 (2003)
3. Nguyen, T, Martin, J, Byrd, E, Embree, N, "Relating Laboratory and Outdoor Exposure of Coatings III. Effect of Relative Humidity on Moisture-Enhanced Photolysis of Acrylic-Melamine Coatings." *Polym. Degrad. Stab.*, **77** 1–16 (2002)
4. Nguyen, T, Martin, J, Byrd, E, "Relating Laboratory and Outdoor Exposure of Coatings IV. Mode and Mechanism for Hydrolytic Degradation of Acrylic-Melamine Coatings Exposed to Water Vapor in the Absence of UV Light." *J. Coat. Technol.*, **75** (941) 37–50 (2003)
5. Keene, LT, Vasquez, MJ, Clayton, CR, Halada, GP, "Failure of Navy Coating Systems 2: Failure Pathways of Artificially Weathered Navy Coating Systems Applied to Chromate Conversion Coated AA2024-T3 Substrates." *Prog. Org. Coat.*, **52** 187–195 (2005)
6. Souto, RM, Gonzalez-Garcia, Y, Gonzalez, S, "Evaluation of the Corrosion Performance of Coil-Coated Steel Sheet as Studied by Scanning Electrochemical Microscopy." *Corros. Sci.*, **50** 1637–1643 (2008)
7. Souto, RM, Gonzalez-Garcia, Y, Gonzalez, S, Burstein, GT, "Imaging the Origins of Coating Degradation and Blistering Caused by Electrolyte Immersion Assisted by SECM." *Electroanalysis*, **21** (23) 2569–2574 (2009)
8. Souto, RM, Gonzalez-Garcia, Y, Gonzalez, S, "Characterization of Coating Systems by Scanning Electrochemical Microscopy: Surface Topography and Blistering." *Prog. Org. Coat.*, **65** 435–439 (2009)
9. Souto, RM, Gonzalez-Garcia, Y, Izquierdo, J, Gonzalez, S, "Examination of Organic Coatings on Metallic Substrates by Scanning Electrochemical Microscopy in Feedback Mode: Revealing the Early Stages of Coating Breakdown in Corrosive Environments." *Corros. Sci.*, **52** 748–753 (2010)
10. Raghavan, D, Gu, X, Nguyen, T, VanLandingham, M, Karim, A, "Mapping Polymer Heterogeneity Using Atomic Force Microscopy Phase Imaging and Nanoscale Indentation." *Macromolecules*, **33** 2573–2583 (2000)
11. Raghavan, D, Gu, X, Nguyen, T, VanLandingham, T, "Characterization of Chemical Heterogeneity in Polymer Systems Using Hydrolysis and Tapping-Mode Atomic Force Microscopy." *J. Polym. Sci. Polym. Phys.*, **39** 1460–1470 (2001)
12. Mansfeld, F, Han, LT, Lee, CC, Zhang, G, "Evaluation of Corrosion Protection by Polymer Coatings Using Electrochemical Impedance Spectroscopy and Noise Analysis." *Electrochim. Acta*, **43** 2933–2945 (1998)
13. Hu, JM, Zhang, JQ, Cao, CN, "Determination of Water Uptake and Diffusion of Cl<sup>-</sup> Ion in Epoxy Primer on Aluminum Alloys in NaCl Solution by Electrochemical Impedance Spectroscopy." *Prog. Org. Coat.*, **46** 273–279 (2003)
14. Miszczyk, A, Darowicki, K, "Accelerated Ageing of Organic Coating Systems by Thermal Treatment." *Corros. Sci.*, **43** 1337–1343 (2001)
15. Rossi, S, Deflorian, F, Fontanari, L, Cambuzzi, A, Bonora, PL, "Electrochemical Measurements to Evaluate the Damage Due to Abrasion on Organic Protective System." *Prog. Org. Coat.*, **52** 288–297 (2005)
16. Hinderliter, BR, Croll, SG, Tallman, DE, Su, Q, Bierwagen, GP, "Interpretation of EIS Data from Accelerated Exposure of Coated Metals Based on Modeling of Coating Physical Properties." *Electrochim. Acta*, **51** 4505–4515 (2006)
17. Oliveira, CG, Ferreira, MGS, "Ranking High-Quality Paint Systems Using EIS. Part I: Intact Coatings." *Corros. Sci.*, **45** 123–138 (2003)
18. Oliveira, CG, Ferreira, MGS, "Ranking High-Quality Paint Systems Using EIS. Part II: Defective Coatings." *Corros. Sci.*, **45** 139–147 (2003)
19. Shao, R, Kalinin, SV, Bonnell, DA, "Local Impedance Imaging and Spectroscopy of Polycrystalline ZnO Using Contact Atomic Force Microscopy." *Appl. Phys. Lett.*, **82** (12) 1869–1871 (2003)
20. O'Hayre, R, Lee, M, Prinz, FB, "Ionic and Electronic Impedance Imaging Using Atomic Force Microscopy." *J. Appl. Phys.*, **95** 8382–8392 (2004)
21. O'Hayre, R, Feng, G, Nix, WD, Prinz, FB, "Quantitative Impedance Measurement Using Atomic Force Microscopy." *J. Appl. Phys.*, **96** 3540–3549 (2004)
22. Darowicki, K, Szocinski, M, Zielinski, A, "Assessment of Organic Coating Degradation Via Local Impedance Imaging." *Electrochim. Acta*, **55** 3741–3748 (2010)
23. Nguyen, T, Hubbard, JB, Pommersheim, JM, "Unified Model for the Degradation of Organic Coatings on Steel in a Neutral Electrolyte." *J. Coat. Technol.*, **68** (855) 45–56 (1996)
24. Sekine, I, "Recent Evaluation of Corrosion Protective Paint Films by Electrochemical Methods." *Prog. Org. Coat.*, **31** 73–80 (1997)